Utilization of ultra-thin n-type Hydrogenated Nanocrystalline Silicon for Silicon Heterojunction Solar Cells

Depeng Qiu, Weiyuan Duan, Andreas Lambertz, Karsten Bittkau, Kaifu Qiu and Kaining Ding

IEK-5 Photovoltaics, Forschungszentrum Jülich GmbH, Wilhelm-Johnen Straße, 52425 Jülich, Germany

***Abstract*—To optimize the electrical performance of silicon heterojunction solar cell devices, the electronic properties and microstructure of n-type nc-Si:H were characterized and analyzed. It was found that higher conductivity and crystalline volume fraction (F_c) of nc-Si:H can be obtained at lower silane gas fraction (f_{SiH4}), lower power and higher phosphorous gas fraction (f_{PH3}). In our case, there is a decline of the passivation for the devices with nc-Si:H after sputtering process. By increasing the phosphine flow fraction, the sputter damage can be reduced and 3%$_{abs}$ gain of *FF* as well as 0.7%$_{abs}$ gain of efficiency is reached compared with reference. The best solar cell exhibits the V_{oc} of 733.3 mV, *FF* of 79.7%, J_{sc} of 39.00 mA/cm^2 and η of 22.79% at the M2 size wafer.**

Keywords— Silicon heterojunction solar cell, Nanocrystalline silicon

I. Introduction

Recently, a certified efficiency (η) of 25.1% was demonstrated for a both sides contacted amorphous silicon/crystalline silicon heterojunction (SHJ) solar cell [1]. However, due to the parasitic absorption in the amorphous silicon (a-Si:H) layers, the SHJ solar cells suffer from lower short-circuit current density (J_{sc}) compared to the conventional diffused homojunction solar cell [2]. In this paper, hydrogenated nanocrystalline silicon (nc-Si:H), a well-recognized material as an alternative window layer to a-Si:H in SHJ solar cells [3-5], was optimized by tuning the process parameters with respect to more conductive layers and high efficiency of devices. To further minimize the parasitic absorption in nc-Si:H and improve the throughput, ultra-thin (5nm) nc-Si:H (n) was used as window layers for the SHJ solar cells in this work.

II. Experimental

The n-type nc-Si:H films in this work were prepared in a plasma enhanced chemical vapor deposition (PECVD) system and the precursor gases are SiH_4, H_2 and PH_3 (=1% diluted in H_2). The samples were deposited at a plasma excitation frequency of 13.56 MHz and a substrate temperature of 200°C. To achieve a high electronic performance, various process parameters like deposition pressure, plasma excitation power and the gas composition were varied. The gas composition is described by the gas fractions for the different gases and defined by $f_{PH3} = [PH_3]/([PH_3] + [SiH_4])$ and $f_{SiH4} = [SiH_4]/([H_2] + [SiH_4])$, where the $[H_2]$, $[PH_3]$ and $[SiH_4]$ are the gas mass flow rate of H_2, PH_3 and SiH_4, respectively. The nc-Si:H films with a thickness of ~35 nm was deposited on Corning 2000 glass, on which 6 nm intrinsic a-Si:H(i) was pre-deposited to ensure similar growth conditions as in the solar cell. A UV-Raman scattering spectroscopy were performed to determine the fraction of crystallites (F_c) of nc-Si:H films [6]. The lateral dark conductivity (σ) of the films was measured by way of two coplanar silver electrodes at room temperature. The textured n-type Czochralski silicon wafers with thickness of 165 µm, resistivity of 1~2 Ωcm and size of M2 (244cm^2) were used for device fabrication. Ozone cleaning procedure and dipping in 1% hydrofluoric (HF) acid were carried out for the wafers, followed by the PECVD depositions of front and rear side silicon stacks. Afterwards, 70 nm indium tin oxide (ITO) layers were prepared on each side of the wafer at a substrate temperature of 200°C by direct current magnetron sputtering. Subsequently, the Ag fingers were printed on both sides of the solar cells by screen printer, followed by a 40-minute annealing treatment at 190°C. The cross-section structure of the rear-junction solar cells is displayed in Fig.1.

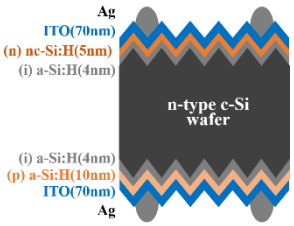

Fig.1: The cross-section structure of the rear-junction solar cells with n-type nc-Si:H thin films.

III. Result and Discussion

A. Material properties

The effects of the deposition parameters on the conductivity (σ) of the nc-Si:H (n) layers are shown in Fig. 2 (a). The dashed line serves as a guide for the eyes. The conductivity increases slightly as reducing the silane gas (f_{SiH4}) fraction from 0.75% to 0.5%. Decreasing the power from 200W to 100W leads to a significant increase of σ by one order of magnitude, from 1.9 S/cm to 22.5 S/cm. Slightly higher conductivity of nc-Si:H, 27 S/cm, was obtained at 4% of f_{PH3} compared with the one at 2%. A reduction of the conductivity can be observed as increasing the deposition pressure from 2.5mbar to 4.5mbar. The nc-Si:H consists of nanocrystalline silicon phases embedded in an amorphous silicon (a-Si:H) matrix [3]. The crystalline phase is

assumed as the percolation paths for the charge carriers transport due to higher effective carrier mobility and doping efficiency than amorphous phase [7, 8]. The crystalline volume fraction was extracted from the UV-Raman spectrum and shown in Fig.2 (b). Increase of the F_c can be found when reducing the f_{SiH4} and plasma generator power, contributed to the increase of the conductivity. Although increasing f_{PH3} from 2% to 4% results in the decrease of F_c, a slight increase of σ can be found in Fig.2 (a), which is due to the higher doping level of the films prepared at higher f_{PH3}.

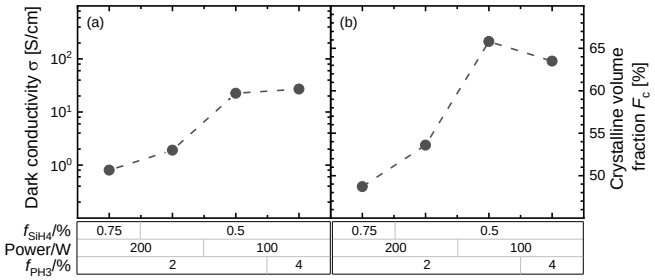

Fig. 2: (a) The dark conductivity and (b) the crystalline volume fraction (F_c) of the nc-Si:H layers prepared under various conditions.

B. *Cell performance*

Figure 3 shows the IV parameters of rear-junction SHJ solar cells with 5nm n-type nc-Si:H layer deposited under various process conditions, which are same as the material development. To make the description easier, we divided the samples into 4 groups and named them as S1, S2, S3 and S4, process details of which can be found in Fig. 3 and Fig. 4. The samples S1, with nc-Si:H prepared at f_{SiH4} of 0.75%, power of 200W and f_{PH3} of 2% are the reference samples.

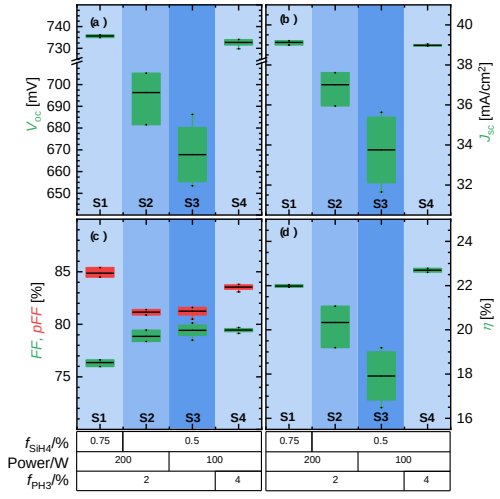

Fig. 3: (a) The open-circuit voltage (V_{oc}), (b) short-circuit current density (J_{sc}), (c) fill factor (*FF*) and (d) power conversion efficiency (η) of the solar cells with n-type nc-Si:H layer prepared at different deposition conditions. The plots summarize the statistic of more than 4 cells per group and the line is the median position.

As decreasing the silane gas fraction from 0.75% to 0.5% or setting the plasma generator power at lower value, a drop of V_{oc} and J_{sc} as well as the pseudo FF can be observed in Fig. 3, which could be due to the passivation issues caused by the deposition processes of nc-Si:H or ITO layers. Nevertheless, there is about 2.5%$_{abs}$ gain of *FF* for S2 and S3 compared with S1. It could be explained by the increase of the dark conductive and crystalline volume fraction for nc-Si:H films prepared at lower silane flow fraction or plasma generator power. Integrating the nc-Si:H films with higher doping concentration (f_{PH3}=4%) in S4, a recovery of the V_{oc} and J_{sc} and slight increase of *FF* can be found comparing with S3. It could be due to the improvement of the carrier collection in the devices. Comparing with the reference, the V_{oc} of S4 is slightly lower, but about 3%$_{abs}$ gain of *FF* is achieved for S4, contributed to the efficiency improvement of 0.7%$_{abs}$. The best solar cell exhibits the V_{oc} of 733.3 mV, *FF* of 79.7%, J_{sc} of 39.00 mA/cm^2 and η of 22.79%.

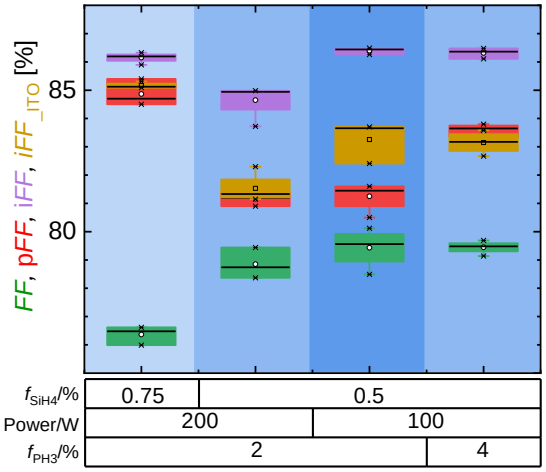

Fig. 4: The *FF*, implied-*FF* before (i*FF*) and after ITO deposition (i$FF_{_ITO}$) and pseudo-*FF* (p*FF*) of the solar cells prepared at different deposition parameters. The implied-FF was evaluated by the Quasi-steady-state photo-conductance (QSSPC) lifetime measurement and pseudo-FF was extracted from the I_{sc}-V_{oc} curves. The plots summarize the statistic of more than 4 cells per group and the line is the median position.

Fig. 4 shows the *FF*, implied-*FF* before (i*FF*) and after ITO deposition (i$FF_{_ITO}$) and pseudo-FF (p*FF*) of the solar cells prepared at deposition parameters S1 to S4. The i*FF* was evaluated by the Quasi-steady-state photo-conductance (QSSPC) lifetime measurement and p*FF* was extracted from the I_{sc}-V_{oc} curves. The i*FF* of S2, measured after the PECVD depositions, are lower than those of the other samples, which could be due to the enhanced hydrogen plasma etching damage on the passivating layers when the silane gas fraction is low [9,10]. By reducing the power of plasma generator, the i*FF* gets higher, indicating the improvement of the passivation. Compared with S3, higher i*FF* is achieved for the S4, which could be because of the enhanced field-effect passivation in S4, attributed to the increase of phosphorous doping concentration. For the S2, S3 and S4, there is a huge gap between the i*FF* and i$FF_{_ITO}$, which demonstrates the serious passivation degradation after the ITO sputtering process, owing to the ion bombardment or light-induced degradation by the Staebler–Wronski effect in a-Si:H [11]. The p*FF* of solar cells show a similar trend as the i*FF* with varying the deposition parameters. From S1 to S4, the gap between p*FF* and *FF* has significantly reduced which means a lower series resistance loss has been achieved after optimizing deposition parameter. This could attribute to the decreased contact resistance between nc-Si:H and ITO which also needs further investigation.

IV. Conclusion

In this work, the material properties of n-type nc-Si:H films were investigated by adjusting the process parameters like power and the gas fraction. Higher conductivity is achieved at lower silane gas fraction, lower power and higher phosphorous gas fraction. Different lifetime degradation after ITO sputtering process was observed for the devices with ultra-thin nc-Si:H (n) layers deposited at various conditions, which could be attributed to the ion bombardment or the ultra-violet radiations during the ITO deposition process. By increasing the phosphine gas fraction a reduction of the sputtering damage was observed, the principle behind which need to be further investigated. Comparing with the reference, there is about $3\%_{abs}$ gain of *FF* for the devices with more conductive nc-Si:H (n) layer, contributed to the efficiency improvement of $0.7\%_{abs}$. The best solar cell exhibits the V_{oc} of 733.3 mV, *FF* of 79.7%, J_{sc} of 39.00 mA/cm^2 and η of 22.79% at the M2 size wafer.

Acknowledgment

The authors would like to thank Hildegard Siekmann for the ITO sputtering, Alain Doumit and Henrike Gattermann for the wafer texture and cleaning, Henrike Gattermann and Klaus Wambach for the screen printing, Silke Lynen, Volker Lauterbach, Andreas Mück, Andreas Schmalen, Johannes Wolff, Daniel Weigand, and Wilfried Reetz for the technical assistance. This work was supported by the German Federal Ministry of Economic Affairs and Energy in the framework of the STREET project (grant: 0324275E), the German Federal Ministry of Economic Affairs and Energy in the framework of the TUKAN project (grant: 0324198D), the German Federal Ministry of Economic Affairs and Energy in the framework of TOUCH project (grant: 0324351) and the (HEMF) Helmholtz Energy Materials Foundry infrastructure funded by the HGF (Helmholtz association). The authors are grateful for the financial support from China Scholarship Council (No. 201706380037) and the wafers supply by LONGI company.

References

[1] D. Adachi et al., “Impact of carrier recombination on fill factor for large area heterojunction crystalline silicon solar cell with 25.1% efficiency,” Appl. Phys. Lett. 107. 233506 (2015).

[2] J. Haschke et al., “Silicon heterojunction solar cells: recent technological development and practical aspects-from lab to industry,” Sol. Energy Mater. Sol. Cell. 187 (2018) 140–153.

[3] O. Vetterl et al., “Intrinsic microcrystalline silicon: A new material for photovoltaics,” Sol. Energy Mater. Sol. Cells, vol. 62, pp. 97–108, 2000.

[4] F. Finger et al., “Improvement of grain size and deposition rate of microcrystalline silicon by use of very high frequency glow discharge,” Appl. Phys. Lett., vol. 65, p. 2588, 1994.

[5] M. Boccard et al., “Multiscale transparent electrode architecture for efficient light management and carrier collection in solar cells,” Nano Lett. vol. 12, pp. 1344–1348, 2012.

[6] C. Wen et al., “Tuning oxygen impurities and microstructure of nanocrystalline silicon photovoltaic materials through hydrogen dilution,” Nanoscale Res. Lett. 9 (2014) 303.

[7] N. Wyrsch et al., “Effect of the microstructure on the electronic transport in hydrogenated microcrystalline silicon,” J. Non-Cryst. Solids, vols. 299–302, Part 1, pp. 390–394, 2002.

[8] H. Kaya et al., “Evaluation of boron and phosphorus doping microcrystalline silicon films,” Jpn. J. Appl. Phys., vol. 23, p. L549, 1984.

[9] J. Geissb¨uhler et al., “Amorphous/crystalline silicon interface defects induced by hydrogen plasma treatments,” Appl. Phys. Lett., vol. 102, p. 231604, 2013.

[10] S. Ghosh et al., “Role of hydrogen dilution and diborane doping on the growth mechanism of p-type microcrystalline silicon films prepared by photochemical vapor deposition,” J. Appl. Phys., vol. 71, p. 5205, 1992.

[11] B. Demaurex, S. De Wolf, A. Descoeudres, Z. C. Holman, and C. Ballif, Appl. Phys. Lett. 101, 171604 (2012).